ChemPubSoc Europe

DOI: 10.1002/cctc.201901719

CHEMCATCHEM Full Papers

Insight into the Nature of Active Species of Pt/Al_2O_3 Catalysts for low Temperature NH_3 Oxidation

Dmitry A. Svintsitskiy,[a, b] Lidiya S. Kibis,[a, b] Andrey I. Stadnichenko,[a, b] Elena M. Slavinskaya,[a, b] Anatoly V. Romanenko,[a] Elizaveta A. Fedorova,[a] Olga A. Stonkus,[a, b] Dmitry E. Doronkin,[c, d] Vasyl Marchuk,[c] Anna Zimina,[c, d] Maria Casapu,[c] Jan-Dierk Grunwaldt,*[c, d] and Andrei I. Boronin*[a, b]

Two series of Pt/γ-Al_2O_3 catalysts for low temperature NH_3 oxidation were prepared using $Pt(NO_3)_4$ and H_2PtCl_6 precursors. Using both precursors results in the formation of small Pt particles ($d < 1.5$ nm), however, Cl-containing Pt precursors give a higher fraction of highly dispersed Pt species. Such species show high stability against thermal or H_2 treatment probably due to the presence of a substantial amount of chlorine on the surface. Treatment of the samples prepared from $Pt(NO_3)_4$ with H_2 leads to the formation of metallic Pt nanoparticles accompanied by the improvement of catalytic activity in NH_3 oxidation at $T < 200\,^{\circ}C$. The main products of ammonia oxidation at temperatures below 250 °C were molecular nitrogen and nitrous oxide with the N_2 selectivity reaching 80%. *Operando* XANES/EXAFS revealed that even after H_2 pretreatment at least 40% of Pt surface remains in oxidized state under reaction conditions resulting in the appearance of N_2O as a by-product.

1. Introduction

The strict environmental protection regulations are currently applied to control the toxic emissions from refineries, power plants, and vehicles.[1,2] Exhausts of many industrial processes such as nitric acid production,[3] biomass and coal gasification,[4] the regeneration of fluid cracking catalysts (FCC),[5] and selective catalytic reduction (SCR) of NO_x by NH_3[6] contain ammonia which has a harmful effect on human health[7,8] and environment.[9] Global NH_3 emission from industry was estimated to be about 220 thousand tons per year.[10] In addition to this, the emerging use of ammonia as an energy carrier for various mobile energy sources and transportation[11–13] also requires solving the NH_3 emission problem preferably via its catalytic transformation to molecular nitrogen.[14]

The catalyst for selective ammonia oxidation is an essential component of NH_3-SCR diesel engine systems for NO_x removal. In these systems NH_3 is generated onboard from aqueous urea solution.[15] For higher NO_x removal efficiency excess of ammonia is dosed resulting in its slip in the exhaust. To remove NH_3 before it reaches the environment the Ammonia Slip Catalyst (ASC) is additionally installed.[16] The state-of-the-art ASC systems include a combination of an ammonia oxidation (AMOX) catalyst (usually, Pt/Al_2O_3) and a SCR catalyst in a dual-layer architecture,[15,17,18] where a part of ammonia is oxidized over the Pt catalyst to N_2 and NO_x, which is further transformed to N_2 over the SCR catalyst layer.

The dual-layer ASC systems have been extensively studied in the last decade. Nevertheless, there is still strong debate on the full understanding of the system, which is required, for example, for the development of the kinetic models,[15] optimization of the catalyst architecture[17] and addressing catalyst deactivation.[19] In addition, further knowledge is necessary to increase the activity of AMOX catalysts to full NH_3 conversion below 250 °C. Among different supported noble metal catalysts, Pt-based systems are considered to be the most active for NH_3 oxidation.[10] However, using Pt-based catalysts requires increasing N_2 selectivity by minimizing the formation of undesired N_2O.[20] Despite many data about NH_3 oxidation to NO_x over single- and polycrystalline platinum surfaces, Pt gauzes or sponges as well as supported platinum

[a] Dr. D. A. Svintsitskiy, Dr. L. S. Kibis, Dr. A. I. Stadnichenko, Dr. E. M. Slavinskaya, Dr. A. V. Romanenko, E. A. Fedorova, Dr. O. A. Stonkus, Prof. A. I. Boronin
Boreskov Institute of Catalysis
Pr. Lavrentieva 5
Novosibirsk 630090 (Russia)
E-mail: boronin@catalysis.ru
[b] Dr. D. A. Svintsitskiy, Dr. L. S. Kibis, Dr. A. I. Stadnichenko, Dr. E. M. Slavinskaya, Dr. O. A. Stonkus, Prof. A. I. Boronin
Novosibirsk State University
Pirogova St. 2
Novosibirsk 630090 (Russia)
[c] Dr. D. E. Doronkin, V. Marchuk, Dr. A. Zimina, Dr. M. Casapu, Prof. J.-D. Grunwaldt
Institute for Chemical Technology and Polymer Chemistry
Karlsruhe Institute of Technology (KIT)
Engesserstr. 20
Karlsruhe 76131 (Germany)
E-mail: grunwaldt@kit.edu
[d] Dr. D. E. Doronkin, Dr. A. Zimina, Prof. J.-D. Grunwaldt
Institute of Catalysis Research and Technology
Karlsruhe Institute of Technology (KIT)
Hermann-von-Helmholtz-Platz 1
Eggenstein-Leopoldshafen 76344 (Germany)

Supporting information for this article is available on the WWW under https://doi.org/10.1002/cctc.201901719

This publication is part of a Special Collection on "Advanced Microscopy and Spectroscopy for Catalysis". Please check the ChemCatChem homepage for more articles in the collection.

catalysts,[3,20–25] the structure-activity relationships for Pt-based systems for selective NH_3 oxidation to N_2 are still under discussion and require further systematic fundamental studies.

The ASCs operate under excess of O_2, which has a great impact on the oxidation state of the active component. Over supported Pt catalysts the main issue to be considered is the relationship between the oxidation state of platinum and its particle size, as they are directly related.[26] Smaller Pt particles are readily oxidized[28,29] and the reducibility of PtO_x species is found to be enhanced with the decrease of particle size.[25,30] It was proposed that metallic Pt is significantly more active for NH_3 oxidation than oxidized platinum,[26–28] which does not provide sites for O_2 dissociation.[5] Due to low resistance to oxidation small Pt nanoparticles are, therefore, considered less active in NH_3 oxidation than larger ones.[25,27,29] The selectivity towards various N-containing products seems to be also governed by Pt particle size and oxidation state.[22,25] The deactivation of platinum is discussed to be caused not only by the noble metal oxidation but also by the accumulation of N-containing surface species, especially at low temperatures.[20,30] Hence, one way to obtain efficient NH_3 oxidation catalysts is to carefully select the Pt precursor[31,32] and the drying/pretreatment procedure,[33–35] since they can influence the size and state of Pt particles. However, the number and nature of active sites are ultimately affected by the changes in reaction conditions.[3,28,36,37] Thus, it is mandatory to establish structure-activity correlations directly during catalyst application to avoid possible modification of the active species due to the sample transfer. The rapid development of *in situ/operando* techniques, which are extensively applied in heterogeneous catalysis nowadays, can provide such an opportunity.[38–40]

This work presents a systematic study of Pt/Al_2O_3 catalysts for low temperature NH_3 oxidation. The size of Pt particles and their oxidation state were varied depending on the Pt precursor and the applied calcination and/or reductive treatment. The outcome of the *operando* X-ray absorption near edge structure (XANES) study allowed us to shed light on the average oxidation state of Pt during the NH_3 oxidation reaction. It was shown that the improvement of catalytic properties at low temperature correlates with the Pt reduction. At higher temperatures, reoxidation of Pt surface takes place leading to the NO_x formation.

2. Results

2.1. Effect of the Pt Precursor

2.1.1. Catalytic Properties

The catalytic properties of the air-calcined and reduced *Pt-N-400* and *Pt-Cl-400* catalysts in the NH_3 oxidation reaction are presented in Figure 1. Such catalysts were prepared using N- and Cl-containing Pt precursors, respectively (see *Experimental section* for details).

All studied catalysts were characterized by the evident consumption/storage of NH_3 from the reaction mixture at room temperature. It resulted in the NH_3 desorption from the catalyst surface at the beginning of heating. Therefore, negative values of NH_3 conversion were observed until the amount of oxidized NH_3 started to exceed the amount of desorbed ammonia. In case of the *Pt-N-400* sample the temperature of 50% conversion of NH_3 (T_{50}) was ca. 230 °C, while the reduction in hydrogen at 250 °C or 600 °C caused the shift of NH_3 conversion curve towards lower temperature reaching the T_{50} value of ~170 °C (Figure 1a). Previously, a similar shift was also observed for Pt/Al_2O_3 catalytic systems in terms of NH_3 oxidation.[5,28] Note that no significant differences in catalytic properties of the *Pt-N-400-250H* and the *Pt-N-400-600H* were observed.

Below 250 °C the main products of NH_3 oxidation over Pt/Al_2O_3 catalysts were N_2 and N_2O. NO and NO_2 appeared in the effluent gas mixture only at temperatures above 250 °C while the N_2 and N_2O concentrations evidently decreased. This distribution of N-containing products depending on the reaction temperature is typical for the Pt-based catalysts.[41,42] The onset of NH_3 conversion for all studied catalysts coincided in temperature with the simultaneous appearance of N_2 and N_2O. It indicates that the same active sites were responsible for N_2 and N_2O formation over Pt/Al_2O_3 surface, possibly, as a result of interaction between N_{ads} and NO_{ads} species on metallic platinum.[3,22] Reduction of the *Pt-N-400* in H_2 at 250 °C resulted in the clear activation of the catalyst in the temperature range from 150 to 200 °C. It was accompanied by the appearance of an additional peak on the N_2O concentration curve (maximum near 180 °C, Figure 1e) with the simultaneous growth of N_2 contribution below 200 °C. Therefore, it confirms the metallic nature of sites for N_2/N_2O formation. Also, note that the H_2 treatment of the *Pt-N-400* sample caused the decrease in NO/NO_2 ratio above 360 °C. It might be due to the change in the average Pt particle size.[25]

In the case of the *Pt-Cl-400* catalyst the T_{50} value of 215 °C was similar to that of the *Pt-N-400*. Reduction of the *Pt-Cl-400* in H_2 at 250 °C did not shift the NH_3 conversion curve and only a slight decrease of the T_{50} value was observed after H_2 reduction at 600 °C (Figure 1b). The N_2, N_2O, NO, and NO_2 concentration curves were rather similar to the as-prepared and reduced *Pt-Cl-400* catalysts (Figures 1d and 1f). It indicates that the H_2 treatment of the *Pt-Cl-400* sample did not significantly modify its catalytic properties in contrast to the *Pt-N-400* catalyst.

2.1.2. Structural Characterization

X-ray diffraction (XRD) data for the *Pt-N* and *Pt-Cl* samples are given in Figure 2. The X-ray diffraction patterns of the pristine *Pt-N-400* and *Pt-Cl-400* catalysts show only reflections stemming from the of γ-Al_2O_3 phase (ICDD PDF-2 # 29-0063). The difference curves of the X-ray patterns of the Al_2O_3 support and Pt-containing samples are given in Figure S1 (*cf. Supporting Information*). Reduction of the *Pt-N-400* with H_2 results in the appearance of small reflections from metallic Pt. Reduction at 600 °C leads to the increase of the Pt particle size. The average size of Pt^0 crystallites determined by the Rietveld method was 1.7 and 3.1 nm for the *Pt-N-400-250H* and *Pt-N-400-600H*

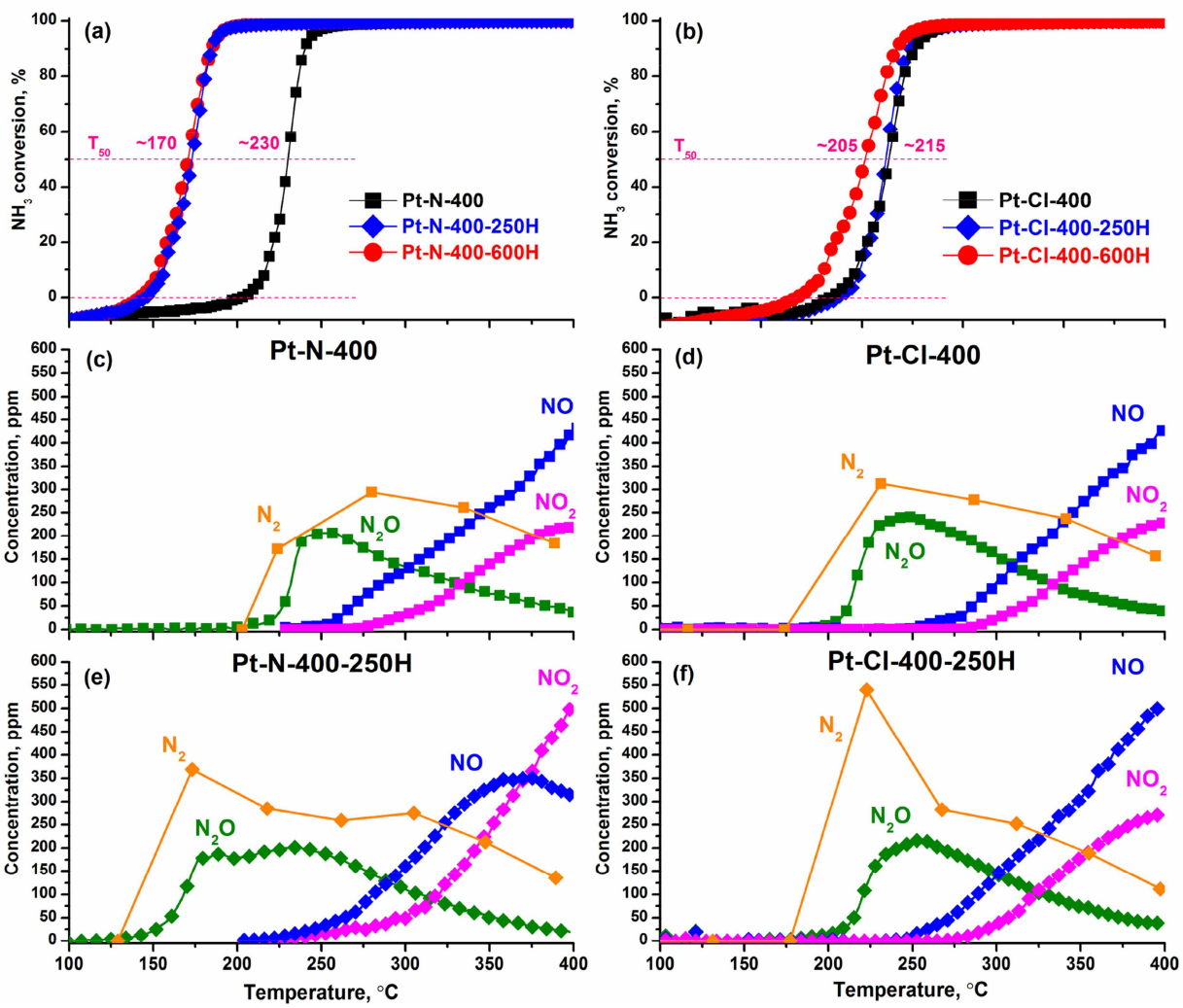

Figure 1. NH_3 conversion over (a) *Pt-N-400* and (b) *Pt-Cl-400* catalysts before and after reduction in H_2 at 250 and 600 °C. Dependence of N_2, N_2O, NO, and NO_2 concentrations on the reaction temperature for (c) *Pt-N-400*, (d) *Pt-Cl-400*, (e) *Pt-N-400-250H*, and (f) *Pt-Cl-400-250H* samples. The reaction mixture contains 0.1 vol.% NH_3 and 4.0 vol.% O_2 (balance He).

samples, respectively. In the case of the *Pt-Cl-400* system no reflections from Pt^0 were observed in the XRD patterns even after H_2 reduction at 600 °C. Hence, all *Pt-Cl* samples contain platinum in a highly dispersed state.

Transmission electron microscopy (TEM) data is in good agreement with the XRD results. The pristine *Pt-N-400* sample contains small Pt particles with an average size of ~1.3 nm (Figure 3e). The reduction of *Pt-N-400* results in the sintering of Pt particles with a bimodal size distribution with maxima around 1.1 and 2.1 nm (Figure 3f). Reduction at 600 °C results in further increase of the particle size up to 1.5–3 nm (Figure S2). Note that the interaction of the *Pt-N* catalyst with $NH_3 + O_2$ mixture up to 400 °C also resulted in a bimodal particle size distribution with maxima of about ~1 and ~2 nm.[28] The *Pt-Cl-400* sample shows very small Pt particles with an average size of about 0.6 nm (Figure 4). Highly dispersed Pt species can be seen as well. Treatment with H_2 at 250 °C causes a negligible increase of the average particle size up to 0.8 nm with the preservation of highly dispersed Pt species. The reduction of the sample at 600 °C results in a slight increase in the average particle size up to 0.9 nm (Figure S2).

2.1.3. X-ray Spectroscopic Investigations

Figure 5 presents the X-ray photoelectron spectra (XPS) of the *Pt-N* (a) and *Pt-Cl* (b) samples. Pt4f spectra can be approximated with two doublet components. For the *Pt-N-400* sample the binding energies (E_b) of $Pt4f_{7/2}$ peaks are 72.2 eV and 74.3 eV. These components can be related to the oxidized species such as $Pt^{\delta+}/Pt^{2+}$ and Pt^{4+}, respectively.[43–45] For the *Pt-Cl-400* sample the $E_b(Pt4f_{7/2})$ value for Pt^{4+}-like component is a bit higher – 74.9 eV. It can be related to the presence of Cl-containing Pt compounds, including oxychlorides PtO_xCl_y.[46] The peak at E_b ($Pt4f_{7/2}$) = 72.2–72.3 eV can also originate from atomically dispersed Pt species.[47] Thus, XPS points to the formation of

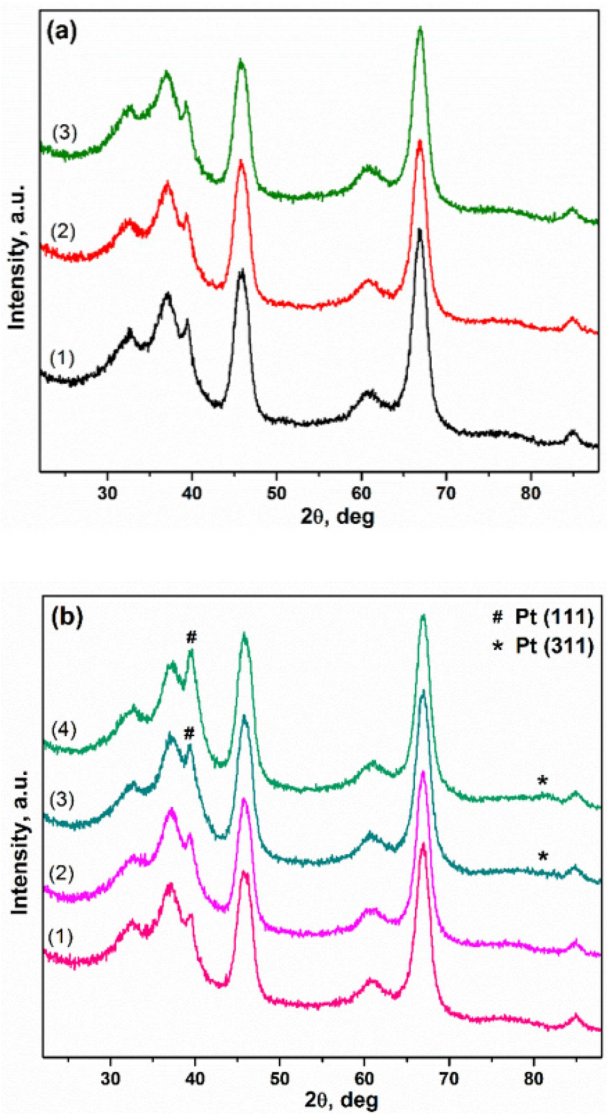

Figure 2. XRD data for (a) the pristine samples: (1) γ-Al_2O_3, (2) *Pt-Cl-400*, (3) *Pt-N-400*; and (b) samples reduced in H_2: (1) *Pt-Cl-400-250H*, (2) *Pt-Cl-400-600H*, (3) *Pt-N-400-250H*, (4) *Pt-N-400-600H*.

oxidized and/or highly dispersed Pt species in the *Pt-N-400* and *Pt-Cl-400* samples. The spectrum of the *Pt-N-400-250H* sample treated with H_2 shows a peak at $E_b(Pt4f_{7/2}) = 71.1$ eV, typical for bulk Pt^0. A slight decrease of the ratio of Pt and Al atomic concentrations (Pt_{at}/Al_{at}) from 1.9% to 1.6% is observed upon reduction of the *Pt-N-400* sample confirming the sintering of the Pt particles (quantitative XPS data for all samples are given in *Supporting Information*, Table S1). The second Pt4f doublet is shifted to lower $E_b(Pt4f_{7/2}) = 73.1$ eV close to $Pt(OH)_2$ and/or PtO species.[48,49] Hence, the treatment of the *Pt-N-400* sample with H_2 results in substantial Pt reduction. In the case of the *Pt-Cl-400-250H* the main $Pt4f_{7/2}$ peak has $E_b(Pt4f_{7/2})$ about 71.9 eV. The increase of the binding energy compared to the value typical for bulk metallic platinum points to the formation of very small metallic (Pt^0) or partially charged ($Pt^{\delta+}$) species. The Pt_{at}/Al_{at} ratio remains about 1.1% for the *Pt-Cl-400* and the *Pt-Cl-400-250H* samples. Based on the XRD and TEM data, we can conclude that the H_2 treatment of the *Pt-Cl-400* sample results in a minor reduction of Pt species without a substantial increase of the particle size. The analysis of the surface composition shows a quite significant amount of chlorine in the *Pt-Cl* samples (see *Table S1*). Only a slight decrease of the Cl_{at}/Al_{at} ratio from 3.7% to 3.3% is observed upon H_2 treatment of the *Pt-Cl-400* sample at 250 °C. The corresponding Cl2p spectra are given in Figure S3. Based on all experimental data, the strong influence of chlorine on the tolerance of Pt species towards reduction and sintering can be reliably concluded. This conclusion is in good agreement with the previous studies on the effect of chlorine on the properties of Pt/Al_2O_3 catalysts.[32,50]

Figure 6 shows (a) XANES and (b) Fourier transformed (FT) extended X-ray absorption fine structure (EXAFS) spectra for the *Pt-N* and *Pt-Cl* samples. Intensity of the first peak above the Pt L_3 absorption edge (so-called "white line", the region marked grey in Figure 6a) is proportional to the density of unoccupied d-states and is often used to estimate oxidation state of Pt[51] by comparing to the reference spectra for PtO_2 and metallic platinum. The intensity of the white line in the *Pt-N-400* XANES spectrum is slightly higher than in the PtO_2 reference spectrum which confirms fully oxidized Pt species. Reduction at 250 °C leads to a significant decrease in the white line intensity in the case of the *Pt-N-400-250H*. Further H_2 treatment at 600 °C leads to even lower white line intensity due to, possibly, sintering of Pt particles and lower availability of Pt surface for interaction with O_2 from the air (note that in this case the reported measurements were performed ex situ).

At the same time, the observed inconsistency between the *Pt-N-400* and PtO_2 XANES spectra, probably due to the different coordination environment around Pt atoms, limits reliable quantification since PtO_2 cannot be used in this case as a good reference for XANES analysis. For this reason, the corresponding EXAFS spectra were also analyzed (Figure 6b).

To further evaluate the structure and quantify the average oxidation state of the Pt sites EXAFS spectra were fitted to a model containing Pt–O and Pt–Pt coordination shells from PtO_2 and the first Pt–Pt coordination shell from metallic Pt (fcc). The average oxidation state of Pt is defined from an average coordination number (CN) in the Pt–O first shell (where CN = 6 corresponds to Pt^{4+}). The fitting results reported in Table 1 confirm full oxidation of the *Pt-N-400* and allow using it as a Pt^{4+} reference for linear combination analysis of XANES spectra. The FT EXAFS spectrum of *Pt-N-400-250H* allows identifying the formation of Pt nanoparticles (backscattering on Pt–Pt shell at an uncorrected distance between 2 and 3 Å) while the *Pt-Cl* samples are largely oxidized and no significant Pt–Pt interaction corresponding to metallic Pt can be identified. Furthermore, both O and Cl nearest neighbors were required to achieve a good EXAFS fit of the *Pt-Cl* samples (Figure S4, Table S2). The reduction of *Pt-Cl-400* sample results in a decrease in the number of chlorine nearest neighbors and an increase of oxygen backscattering.

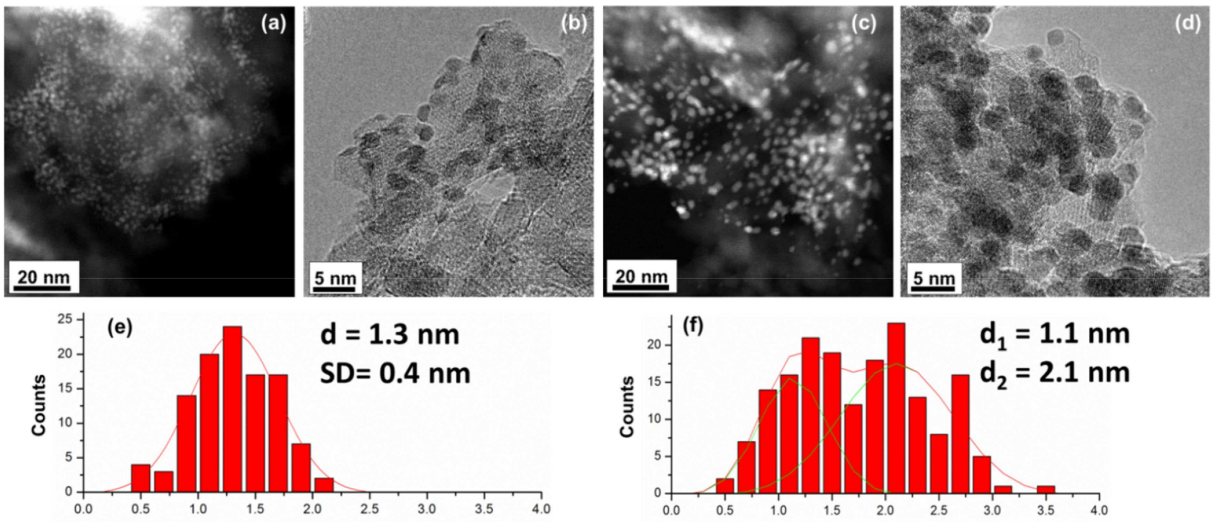

Figure 3. HAADF-STEM and TEM data for (a,b) *Pt-N-400* and (c,d) *Pt-N-400-250H* samples. Particle size distribution for (e) *Pt-N-400* and (f) *Pt-N-400-250H* samples with total number of particles near 100–150.

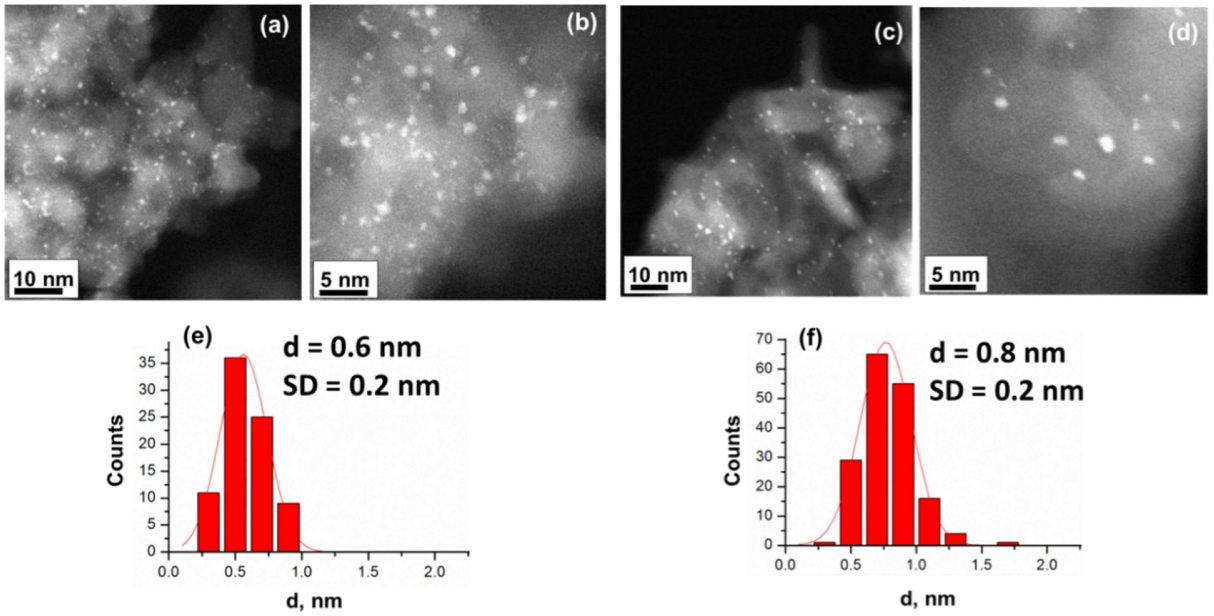

Figure 4. HAADF-STEM data for (a,b) *Pt-Cl-400* and (c,d) *Pt-Cl-400-250H* samples. The particle size distribution for (e) *Pt-Cl-400* and (f) *Pt-Cl-400-250H* samples with total number of particles near 100–150.

Table 1. A summary of average Pt oxidation states and coordination environments determined from XANES and EXAFS spectra.

Catalyst	Pt oxidation state	Pt–O [Cl] distance [Å]	CN	Pt–Pt [metallic] distance [Å]	CN	Pt–O [Cl]	Pt–Pt [metallic]	ρ [%]
Pt-N-400	+4±0.7[a]	1.99±0.01 (O)	6.0±1.0 (O)	n.a	n.a	2.1±2.0	9.2±1.7	0.8
Pt-N-400-250H	+1.01±0.7[a]	1.97±0.02 (O)	1.9±0.5 (O)	2.74±0.02	6.0±2.3	4.2±4.3 (O) 9.8±3.7 (Pt)	7.0±2.1	1.6
Pt-Cl-400	–	2.00 (O) 2.27±0.06 (Cl)	3.0±0.5 (O) 2.3±3.0 (Cl)	n.a.	n.a.	7.0±10.8	10.3±5.4	4.3
Pt-Cl-400-250H	–	2.00 (O) 2.29±0.04 (Cl)	3.6±1.0 (O) 1.5±1.0 (Cl)	n.a.	n.a.	2.8±6.9	9.2±2.4	1.0

[a] Determined by linear combination analysis (LCA) of XANES spectra using *Pt-N-400* and Pt foil spectra as references for Pt^{4+} and Pt^{0} respectively in the range 11545–11595 eV. In lieu of Pt oxychloride reference spectra, LCA of Pt–Cl samples was not performed.

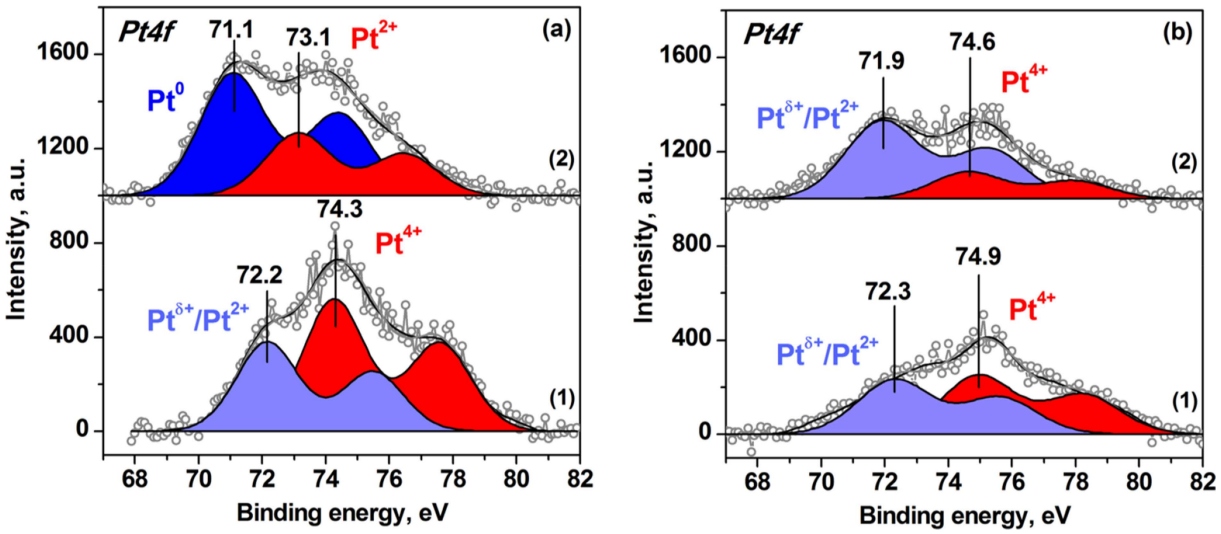

Figure 5. Pt4f spectra for (a) *Pt-N* samples: (1) *Pt-N-400*, (2) *Pt-N-400-250H*; (b) *Pt-Cl* samples: (1) *Pt-Cl-400*, (2) *Pt-Cl-400-250H*. Blue-and red-colored peaks corresponds to metallic and oxidized platinum, respectively.

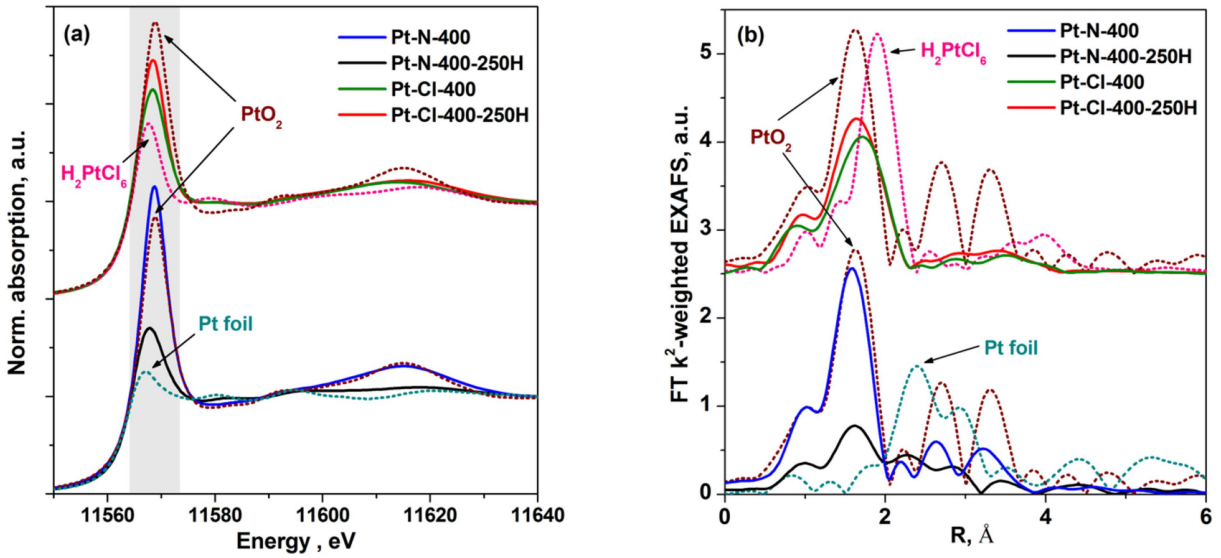

Figure 6. (a) *Ex situ* XANES (grey field marks the "white line" peak) and (b) FT EXAFS (uncorrected for the phase shift) spectra of *Pt-N-400*, *Pt-N-400-250H*, *Pt-Cl-400*, *Pt-Cl-400-250H*, and data for PtO_2, metallic *Pt* and H_2PtCl_6 reference samples. The k-range of EXAFS of 2.5-10.5 $Å^{-1}$.

2.2. Activation of Pt-Cl Catalysts by High-Temperature Treatment

2.2.1. Catalytic Properties

Figure 7 presents the catalytic data for NH_3 oxidation over the *Pt-Cl* catalysts calcined at different temperatures, namely: *Pt-Cl-400*, *Pt-Cl-600,* and *Pt-Cl-800* catalysts. In contrast to H_2 reduction at 600 °C, calcination in air at elevated temperature resulted in the improvement of catalytic activity accompanied by a shift of the NH_3 conversion curve towards lower temperatures – to 190 °C and 170 °C for the *Pt-Cl-600* and *Pt-Cl-800* catalysts, respectively. In the case of the *Pt-Cl-800* sample an additional peak appeared on the N_2O concentration curve in the range 150–200 °C indicating the formation of additional active sites for NH_3 oxidation to N_2/N_2O. It is known that calcination at temperature above 600 °C causes decomposition of oxidized Pt species to metallic Pt particles.[52,53] Based on the literature data, we can propose that calcination of our samples at 800 °C should result in the decomposition of PtO_x and/or PtO_xCl_y species. The enhanced tolerance of such particles toward oxidation under reaction conditions is likely to be caused by their large size. The appearance of reduced/metallic Pt species was also accompanied by the increase in NO_2 production at high temperatures as observed for the reduced *Pt-N-400* catalyst (Figure 1e).

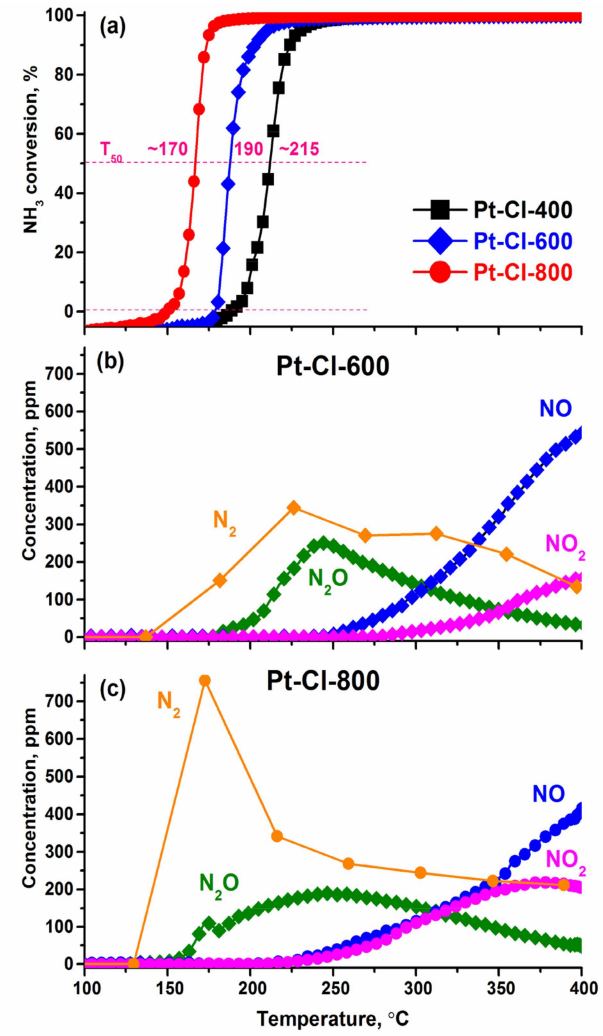

Figure 7. (a) NH_3 conversion profiles over *Pt-Cl-400*, *Pt-Cl-600* and *Pt-Cl-800* catalysts. The dependence of N_2, N_2O, NO, and NO_2 concentrations on the reaction temperature for (b) *Pt-Cl-600* and (c) *Pt-Cl-800* samples. The reaction mixture contains 0.1 vol.% NH_3 and 4.0 vol.% O_2 (balance He).

2.2.2. Structural Characterization

XRD patterns for the *Pt-Cl* samples calcined at $T \geq 600\,^{\circ}C$ show the reflections stemming from metallic Pt (Figure 8). The average size of Pt^0 particles is about 18 and 50 nm for the *Pt-Cl-600* and *Pt-Cl-800* samples, respectively. Note that in the case of the *Pt-Cl-600* the amount of crystalline Pt^0 particles is small in contrast to the *Pt-Cl-800* sample.

TEM data also show the gradual increase of the particle size with calcination of the *Pt-Cl* sample at higher temperatures (Figure 9). For the *Pt-Cl-600* sample Pt particles with size of about 0.7 nm and no highly dispersed Pt species can be detected (Figure 9c). In the case of the *Pt-Cl-800* sample only large particles with size about 30–200 nm can be seen without the presence of highly dispersed Pt species. Hence, calcination of the *Pt-Cl* catalyst at 600 °C does not cause significant Pt sintering. The major part of platinum remains in a dispersed state.

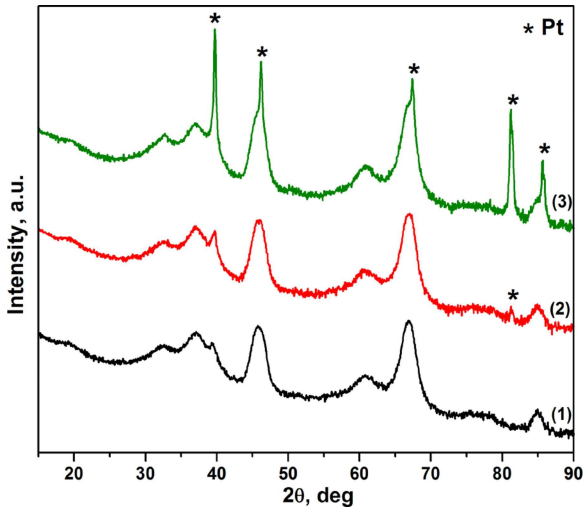

Figure 8. XRD patterns for the (1) *Pt-Cl-400*, (2) *Pt-Cl-600*, and (3) *Pt-Cl-800* samples.

2.2.3. X-ray Photoelectron Spectroscopy

Two doublet components with $E_b(Pt4f_{7/2})$ at 72.1 and 74.8 eV corresponding to $Pt^{\delta+}/Pt^{2+}$ and Pt^{4+} species can be observed in the Pt4f spectrum of the *Pt-Cl-600* sample (Figure 10). Thus, calcination of the *Pt-Cl* sample at 600 °C does not substantially change the oxidation state of platinum. Note, that the surface amount of chlorine is still high for the *Pt-Cl-600* sample reaching Cl_{at}/Al_{at} ratio of 1.9% (Figure S3). However, for the *Pt-Cl-800* sample a substantial reduction of platinum is observed. The E_b ($Pt4f_{7/2}$) of the main peak is 71.3 eV which is close to the bulk metallic platinum, and its contribution is about 80% of the overall Pt4f signal intensity. So, air-calcination at 800 °C results in the substantial reduction and sintering of Pt species. However, a decrease of the Pt surface concentration is observed upon calcination at 800 °C. The Pt_{at}/Al_{at} ratio decreases to ~0.5% for the *Pt-Cl-800* sample due to the sintering of Pt particles. Also, calcination at 800 °C leads to a substantial decrease of surface Cl concentration (Figure S3) indicating again the significant role of Cl for the preservation of platinum in the highly dispersed state.[32,54] For the Pt nitrate-derived samples, calcination already at 600 °C caused decomposition of oxidized Pt species and sintering of the Pt nanoparticles.[55]

2.3. *Operando* XANES under $NH_3 + O_2$ Conditions

In order to analyze the role of Pt state in catalytic NH_3 oxidation, the catalytic experiments were complemented by *operando* XANES. Figure 11 reports average oxidation state of Pt (probed in the first quarter near the inlet of the catalyst bed) as well as the simultaneously recorded catalytic data (conversion of NH_3 and yields of N_2, N_2O, and NO_x) for the *Pt-N-400* and *Pt-N-400-250H* catalysts during the first and second heating in the $NH_3 + O_2$ mixture. The absolute error of Pt oxidation state values determined by linear combination analysis with *Pt* and *PtO_2*

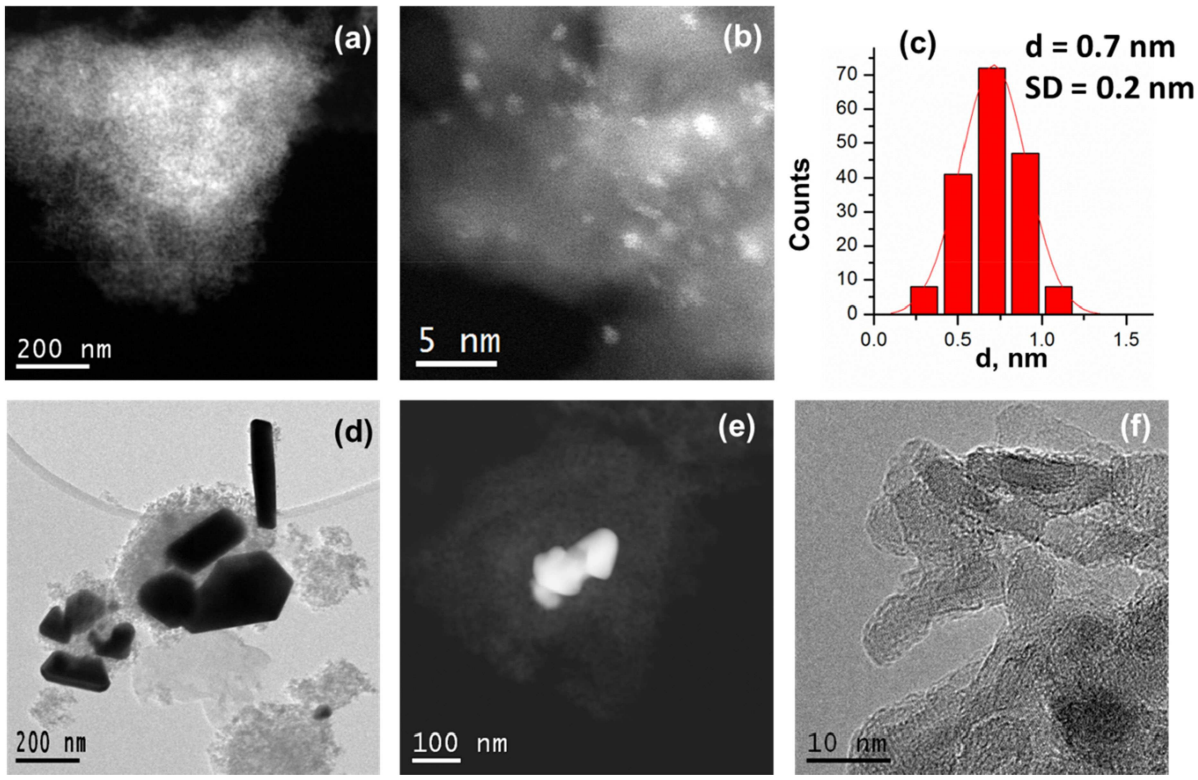

Figure 9. HAADF-STEM and HRTEM data for (a,b) *Pt-Cl-600* and (d-f) *Pt-Cl-800* samples. Particle size distribution for the (c) *Pt-Cl-600* sample with the total number of particles near 150.

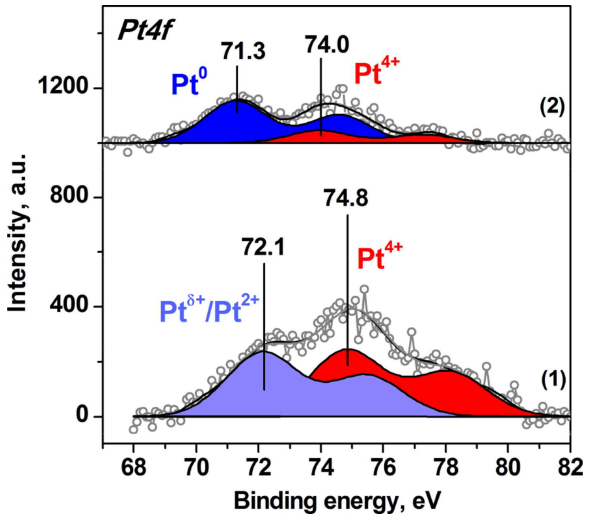

Figure 10. Pt4f spectra for (1) *Pt-Cl-600*, (2) *Pt-Cl-800* samples. Blue-and red-colored peaks correspond to metallic and oxidized platinum, respectively.

references can reach 10% while the fits relative to the first and the last spectrum have relative error values of less than 2%, and thus the reported trends are rather precise.

It should be noted that there are some differences in the onset temperature, T_{50} values, and product yields if we compare results of catalytic tests in a plug flow lab reactor and the plug flow microreactor used during the operando XANES experiments. These differences might be explained by the different conditions of the experiments: reactor configurations, gas hourly space velocity, temperature ramp rate, sample loading, etc. Hence, a direct comparison of the catalytic data is not possible. However, the catalytic profiles detected during operando XANES are helpful for the correlation of the average oxidation state of Pt with the NH_3 conversion and for deriving qualitative trends in the reaction product yields.

When comparing the first and the second heating light-off of the *Pt-N-400* catalyst, the average oxidation state of Pt changes drastically from approx. +3.75 to less than +2. At the same time, the NH_3 conversion curve is only slightly (<20 °C) shifted to lower temperatures and the selectivity trends are not significantly influenced.

Pretreatment of the *Pt-N-400* with H_2 results in a pronounced increase of NH_3 conversion at temperatures below 250 °C, in a good agreement with the catalytic data obtained in the laboratory test bench (plug flow reactor, Figure 1). The reductive pretreatment causes the decrease of the average Pt oxidation state down to +1.2 with its variation in +0.7–+1.2 range during heating under NH_3+O_2 conditions. The prereduced *Pt-N-400-250H* catalyst is characterized by Pt reduction at intermediate temperatures (corresponding to offset of NH_3 conversion) and a slight increase in the Pt oxidation state at higher temperatures (Figure 11c,d). A similar but less pronounced trend is observed for the second heating of the *Pt-N-400* sample in the reaction mixture (Figure 11b). This may be a

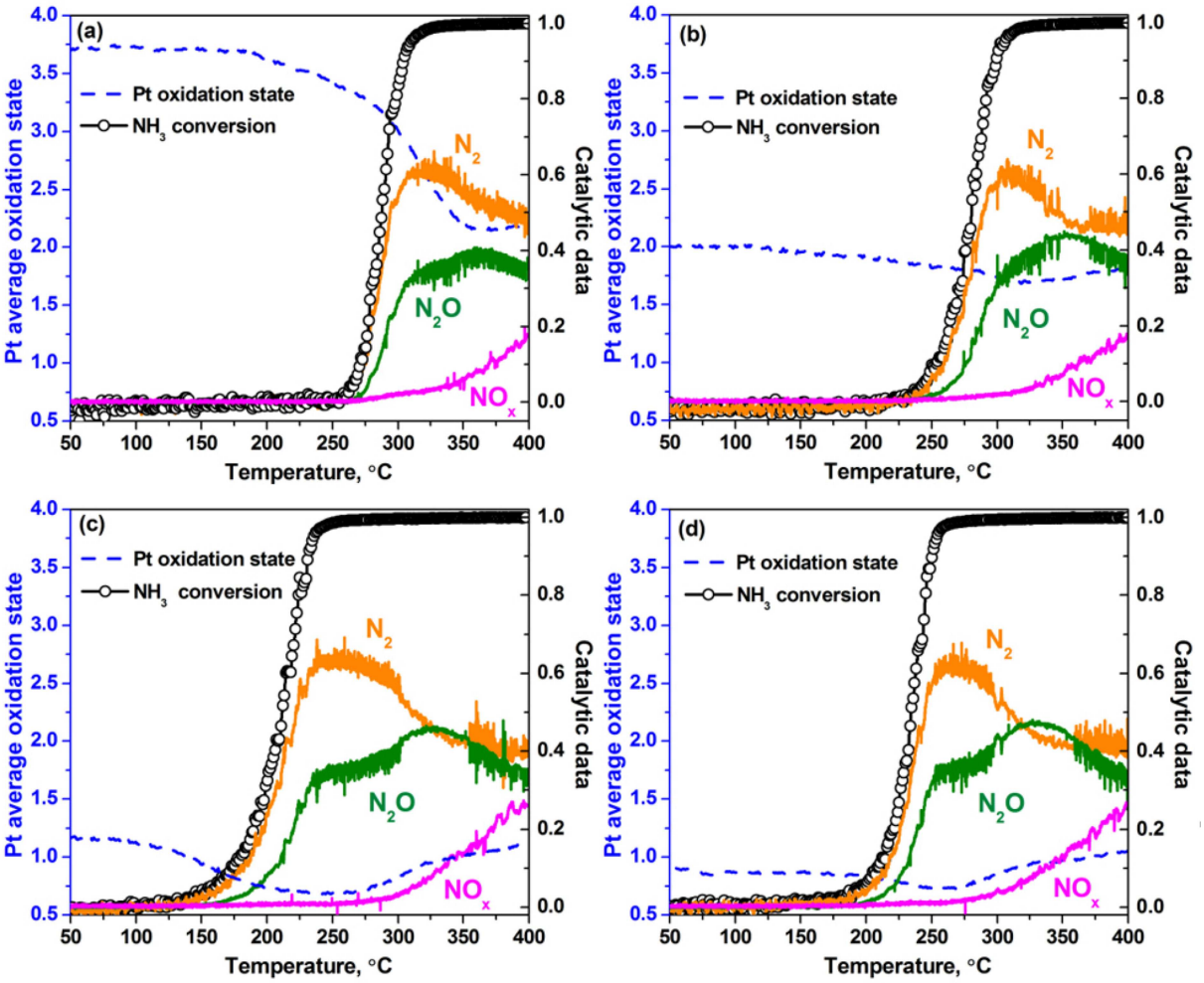

Figure 11. NH_3 conversion, N_2, N_2O, and NO_x yields, and Pt average oxidation state profiles obtained from *operando* XANES experiments during (a) the first and (b) second heating of *Pt-N-400*, and (c) the first and (d) second heating of *Pt-N-400-250H*. The average Pt oxidation state was determined by a linear combination analysis of the XANES spectra using internal references from QEXAFS datasets in a fitting range of 11544–11594 eV.

sign of surface-oxidized Pt nanoparticles being reduced by NH_3 during the reaction onset with further chemisorption of oxygen at higher temperatures. Due to the high NH_3 conversion at high temperature, the NH_3 concentration in the gas phase is not sufficient to remove surface oxygen causing Pt oxidation. Similar behavior of Pt NPs was observed in CO oxidation.[56] The lowest value of Pt oxidation state in the case of the *Pt-N-400-250H* catalyst ~ +0.7–+0.8 corresponds to the reaction temperature of 180–250 °C. After this treatment NH_3 conversion reaches ca. 100% and only N_2 and N_2O appear as reaction products. It indicates that reduced Pt species are mainly responsible for low temperature NH_3 oxidation. Furthermore, we can observe that the steady-state value of the average Pt oxidation state is close to +0.9±0.2. In the case of *Pt-N-400* catalyst, this value was not reached during the first and the second heating-cooling cycles due to the low rate of Pt oxidation/reduction.[57,58]

During the *operando* XANES study the N_2, N_2O, and NO_x formation trends were similar for the *Pt-N-400* and *Pt-400-250H* catalysts and, hence, independent on the average oxidation state of Pt. The only difference is in the light-off temperature. Also, the NO_x contribution at high temperatures is slightly larger in the case of catalyst with more reduced Pt (Figure 11c,d). This agrees well with the catalytic data obtained in the plug flow reactor (Figure 1). Hence the overall rate of NH_3 oxidation is probably related to Pt oxidation state, which should be completely metallic to reach the highest catalytic activity. However, the steady-state Pt oxidation state which can be reached in the presence of O_2 excess in the reaction mixture for the NPs of 1–2 nm is only ~0.7–0.8. The remaining oxygen coverage on Pt surface leads to the appearance of N_2O in addition to N_2 at temperatures <250 °C. Note that the Pt reoxidation under the reaction conditions above 250 °C (Figure 11) is accompanied by the decrease of the selectivity towards N_2 formation and an increase in NO_x formation.

3. Discussion

Two Pt/Al_2O_3 systems were thoroughly investigated by a systematic variation of the pretreatment and the combination of physicochemical techniques (XRD, XPS, *operando* XANES/EXAFS, TEM) to unravel the relationship between Pt state, particle size and catalytic properties in NH_3 oxidation. The two sets of Pt/Al_2O_3 catalysts were prepared by incipient wetness impregnation using $Pt(NO_3)_4$ and H_2PtCl_6 precursors.

Calcination in air and reduction with H_2 at different temperatures were applied to control the oxidation state and particle size of Pt. Pristine Pt/Al_2O_3 catalysts calcined at 400 °C comprised of highly dispersed and deeply oxidized (Figure 5, Table 1) Pt nanoparticles with an average size less than 2 nm. Such particles exhibit significant catalytic activity in NH_3 oxidation only above 200 °C with the formation of N_2/N_2O (at $T < 250$ °C) and $N_2/N_2O/NO/NO_2$ (at $T > 250$ °C) reaction products (Figure 1). H_2 treatment of Pt/Al_2O_3 prepared from the $Pt(NO_3)_4$ precursor results in (1) the significant reduction of Pt (Table 1), (2) the appearance of bimodal particle size distribution with maxima at ~1 and ~2 nm (Figure 3), and (3) the enhancement of the NH_3 oxidation activity at temperature below 200 °C. Such an enhancement is accompanied by the evident widening of the temperature window of N_2/N_2O formation by 50–60 °C (Figure 1). The improvement of the catalytic activity in NH_3 oxidation for pre-reduced catalysts is well-known for Ag-[59,60] and Pt-based[30,61] systems owing to the generation of metallic species, which facilitate the adsorption and dissociation of NH_3 in the presence of O_2. H_2 treatment at high temperature (600 °C) results in the increase of average Pt particle size (up to ~3 nm) without significant changes in the catalytic properties. It indicates that Pt oxidation state is of primary importance for NH_3 oxidation while the effect of Pt particle size is only related to the stabilization of metallic platinum under O_2-rich conditions.[27,28,62]

In the case of Pt/Al_2O_3 catalysts prepared from H_2PtCl_6 precursor the treatment with H_2 does not improve the catalytic activity at $T < 200$ °C due to the stabilization of highly dispersed (< 1 nm, Figure 4) and oxidized Pt clusters (Table 1). It might be related to the residual Cl on the catalyst surface (Table S1). From the XPS data presented in Figure 5b, the presence of PtO_xCl_y with $E_b(Pt4f_{7/2}) > 74.5$ eV was revealed in the pristine samples as well as catalysts after the H_2 treatment. Platinum oxychlorides PtO_xCl_y interact stronger with alumina surface than PtO_x species resulting in the stabilization of highly dispersed particles.[63] Additionally, the presence of Cl might be responsible for the redispersion of Pt particles at high temperatures.[32] The influence of Cl on the catalytic properties of Pt/Al_2O_3 was discussed in terms of CH_4 oxidation[50,63] and the decrease of catalytic activity for Cl-containing Pt/Al_2O_3 catalysts was suggested to be a result of the preservation of oxidized Pt state hindering CH_4 adsorption. Similarly, oxidation of Pt might have a negative effect on the adsorption of NH_3. The ammonia adsorption followed by its activation by adsorbed oxygen is considered as the rate-determining step of catalytic NH_3 oxidation over platinum at low temperatures.[22,41] EXAFS data confirm the presence of Cl and O neighbors in the first coordination shell of Pt, which explains the significantly higher Pt oxidation state in the reduced Pt/Al_2O_3 catalysts in contrast to Cl-free samples (Table 1). Therefore, Cl-containing Pt/Al_2O_3 catalysts are not active in NH_3 oxidation below 200 °C due to the preservation of oxidized Pt species, which are unable to adsorb and activate ammonia. Only calcination at 600–800 °C causes the removal of Cl from Pt/Al_2O_3 (Table S1) resulting in the appearance of large Pt^0 particles with improved catalytic activity in NH_3 oxidation at $T < 200$ °C (Figure 7). Finally, the residual Cl might also influence the acidity of catalyst surface resulting in the modification of the catalytic properties.[63,64] In the present study Cl-containing and Cl-free Pt/Al_2O_3 catalysts were characterized by similar amount and strength of acidic sites adsorbing NH_3 at $T > 150$ °C (*cf. Supporting Information*), i.e. temperature at which the NH_3 conversion was observed (Figures 1 and 5). Hence, it can be suggested that the modification of the surface acidity for Pt/Al_2O_3 by Cl has a negligible effect on catalytic NH_3 oxidation.

The treatment of the Cl-free Pt/Al_2O_3 samples with H_2 causes a significant enhancement of its catalytic activity in NH_3 oxidation (Figure 1a) while the consequent heating-cooling cycles in $NH_3 + O_2$ mixture up to 400 °C have a little effect on its performance (Figure 11). According to the *operando* XANES data, the H_2 treatment results in the decrease of average Pt oxidation state, which, then, varies between +0.7–+1.2 under $NH_3 + O_2$ conditions (Figure 11). Based on the TEM, XPS and XANES data we can speculate on the ratio of metallic and oxidized Pt atoms on the surface of the *Pt-N-400-250H* sample vs. bulk species. Taking into account the Pt particle size distribution, which is the same before and after catalytic measurements,[28] the fraction of surface Pt atoms for this sample can be estimated to be ~62% (*cf. Supporting information*). As indicated by the XPS data only Pt^0 and Pt^{2+} oxidized species are present on the surface of this sample (Figure 5a). Therefore, oxidation of all surface Pt atoms (~62%) to Pt^{2+} state would give the average Pt oxidation state ~ +1.25 rather close to value initially observed for this sample by XANES (Figure 11). It indicates that the interaction of prereduced Pt particles with oxygen leads to nearly complete oxidation of their surface, in good agreement with previously published data.[62] During catalysis in $NH_3 + O_2$ mixture at $T < 250$ °C the decrease of the average Pt oxidation state down to ~ +0.7 is observed. Note that this value might be related to the contribution of both Pt^{2+} and Pt^{4+} surface species. According to the literature data, the stoichiometry of the surface PtO_x structures upon heating in O_2 depends on the Pt particle size with x value changing from 1 to 2 when particle size decreases below 2 nm.[65] Taking into account the size distribution of Pt particles for the *Pt-N-400-250H* sample we can estimate the maximal Pt oxidation state assuming that initial Pt^0 nanoparticles are oxidized to PtO_x structures. The integration of the particle size distribution function with the corresponding limits (*cf. Supporting Information*) gives the maximal Pt oxidation state in the case of *Pt-N-400-250H* catalyst close to ~ +2.9. Thus, the minimal value of Pt oxidation state observed during catalysis (~ +0.7) corresponds to oxidation of ~25% of all Pt atoms or ~40% of Pt surface. Based on the obtained results we can conclude that for the Pt/

Al_2O_3 samples containing 1–2 nm Pt particles at least 40% of surface Pt atoms would be oxidized under NH_3 oxidation conditions irrespective to the pretreatment procedure.

In accordance with the previously proposed mechanism of NH_3 oxidation over platinum,[3,22,30] the appearance of N_2O as a reaction product is inevitable in the presence of O_2 excess even at low temperatures due to high degree of Pt oxidation. It was claimed that deactivation of Pt/Al_2O_3 in the catalytic NH_3 oxidation occurs at temperatures below 130 °C due to the accumulation of NH_x species on the Pt surface while adsorbed oxygen species cause deactivation at higher temperatures.[20] The presented *operando* XANES data demonstrate that in the case of highly dispersed Pt particles the stabilization of PtO_x species on the platinum surface takes place in the whole temperature range of interest up to 400 °C (Figure 11). Similar behavior was established during mathematical simulations of Pt-based diesel oxidation catalysts under lean conditions.[57,66] The surface coverage of PtO_x was found to vary from 0.3 to 0.8 depending on the reaction temperature. The lowest PtO_x coverage corresponded to the highest catalytic activity which can be reached below 200 °C due to Pt reduction or above 400 °C as a result of PtO_x decomposition.[57] In the case of NH_3 oxidation the best catalytic performance is attributed to metallic Pt species providing sites for NH_3 and O_2 adsorption followed by ammonia activation.[5,27,41] Therefore, the degree of Pt surface oxidation should be controlled to tune the catalytic properties of Pt-based systems in NH_3 oxidation including selectivity to desired reaction products.[22,25]

The most appropriate way to control Pt oxidation is a variation of Pt particle size. Larger Pt particles tend to be less oxidized while smaller PtO_x structures require higher temperatures to be reduced to Pt^0.[26,67] The optimal Pt particle size for low temperature NH_3 oxidation was discussed to be in the range from 2–4 to 20 nm.[25,27] In the present work no significant difference in the NH_3 oxidation rate is found for Pt/Al_2O_3 catalysts with the average Pt particle size more than 2 nm (Figures 1 and 7). The highest oxidation rate is reached already for the prereduced 1–2 nm Pt particles. However, the N_2 selectivity for such particles does not exceed 60–70% (Figures 1 and 11) due to the presence of at least 40% of the oxidized Pt species on the noble metal particle surface under reaction conditions. To enhance the N_2 selectivity the steady-state oxygen concentration on Pt surface under reaction conditions has to be decreased. Therefore, the stabilization of Pt particle size above 2 nm with narrow size distribution should be considered as a subject for further research with the aim to improve the catalytic properties of Pt-based catalysts in selective NH_3 oxidation at low temperatures.

4. Conclusions

Platinum supported on Al_2O_3 is considered as the most appropriate system for selective NH_3 oxidation among various ammonia slip catalytic systems. In this work Pt/Al_2O_3 catalysts prepared by impregnation using $Pt(NO_3)_4$ and H_2PtCl_6 precursors were investigated by *ex situ* and *operando* spectroscopy to establish a relationship between the Pt oxidation state, the particle size and the catalytic properties in NH_3 oxidation. In the presence of O_2 excess in the reaction mixture the main products of NH_3 oxidation were N_2 and N_2O below 250 °C, while NO and NO_2 appeared at higher temperatures. It was shown that the nature of the Pt-containing precursor has a strong impact on the size of the obtained Pt nanoparticles as well as on their redox properties. The presence of residual Cl on the catalyst surface provided enhanced tolerance towards sintering and reduction of Pt during calcination and H_2 treatment, respectively. The preservation of highly dispersed oxidized Pt nanoparticles due to residual Cl was proposed to be responsible for the low catalytic activity in NH_3 oxidation below 200 °C. Using a Cl-free Pt precursor during the synthesis of Pt/Al_2O_3 catalysts allowed stabilizing 1–2 nm Pt particles. The reduction of such particles with H_2 leads to the formation of metallic Pt species with improved catalytic activity in NH_3 oxidation at $T < 200$ °C. *Operando* XANES study revealed the variation of the average Pt oxidation state depending on the reaction temperature during catalytic NH_3 oxidation. It was found that the highest N_2 selectivity is observed in the temperature range corresponding to the most reduced Pt surface. However, a substantial part of Pt surface remains in oxidized form as PtO_x under $NH_3 + O_2$ conditions limiting the N_2 selectivity. To further tune the catalytic properties of Pt/Al_2O_3 catalysts in NH_3 oxidation optimization of Pt particle size is required. The size of Pt particles should be large enough to prevent oxidation under reaction conditions with O_2 excess, while the upper limit of Pt particle size is defined by the requirement to efficiently use the expensive active component of the catalysts.

Experimental Section

Sample Preparation

Boehmite AlO(OH) (Pural SCF-55, Sasol, Germany) was calcined in static air at 750 °C for 4 h (heating ramp 5°/min with intermediate calcination at 300 °C for 1 h) to obtain γ-Al_2O_3 support. The specific surface area of the prepared alumina as determined by BET was 174 m^2/g. 2 wt.% Pt was deposited by incipient wetness impregnation with aqueous solutions of $Pt(NO_3)_4$ or H_2PtCl_6. Then the samples were dried for 16 h at room temperature followed by heating to 60 °C for 1 h and further to 120 °C for 2 h. Finally, the catalysts were calcined in air at 400, 600 or 800 °C for 4 h. Some samples were additionally reduced in H_2 flow at 250 or 600 °C for 2 h. Samples are designated depending on the Pt precursor (N stands for the nitrate and Cl – for chloride) and pretreatment conditions. For instance, the designation "*Pt-N-400-250H*" corresponds to a Pt/Al_2O_3 sample prepared from $Pt(NO_3)_4$, calcined in air at 400 °C followed by the reduction in H_2 at 250 °C.

X-ray Diffraction

X-ray diffraction (XRD) patterns were obtained on a Bruker D8 diffractometer (Germany) using Bragg-Brentano geometry, CuK_α radiation, and a Ni filter in the reflected beam path to remove the CuK_β component. The primary slit was 0.1°, the receiving one was 2.2°, the aperture of the Soller slits in the primary and reflected beams was 2.5°. The diffraction intensities were measured using an

one-dimensional LynxEye detector with an angular range of 2.9° on a 2θ scale. XRD patterns were collected in the 2θ range 15–90° with a 0.05° step and acquisition time of 5 s. ICDD PDF-2 powder database was used for the analysis of the crystalline phases. The structure refinement and profile analysis were carried out with the TOPAS software package.[68] The X-ray diffraction patterns for Pt/Al_2O_3 samples were refined as a set of reflections from γ-Al_2O_3 with fixed parameters (defined from a measurement of the pristine support) and metallic platinum using the Rietveld method. To estimate the instrumental broadening crystalline Si powder was used as a reference. The mean crystallite size was calculated using the LVol-IB method.[68]

Transmission Electron Microscopy

The data were collected on a JEM-2200FS electron microscope (JEOL Ltd., Japan) with an accelerating voltage of 200 kV to obtain high-resolution TEM and STEM HAADF images with a spatial resolution of 1 Å. Images of crystal lattices obtained by high-resolution transmission electron microscopy were analyzed by the Fourier method. The samples were dispersed in ethanol ultrasonically and deposited by sputtering the ethanol dispersion on 3 mm copper grids covered with a carbon film. The particle size distribution was determined from the TEM data using ImageJ software.[69]

X-ray Photoelectron Spectroscopy

X-ray photoelectron spectra (XPS) were measured on an ES300 spectrometer (KRATOS, UK) using MgKα source (1253.6 eV). The $Au4f_{7/2}$ and $Cu2p_{3/2}$ core-level spectra of gold and copper foils with binding energy (E_b) at 84.0 eV and 932.7 eV were used for the spectrometer calibration. The maximum of the Al2p line set at 74.5 eV was used as an internal standard for calibration of the experimental spectra. Pt4f spectra were analyzed after the subtraction of the Al2p signal. The Al2p, Pt4f, C1s, O1s, Cl2p core level spectra were used for the analysis of surface composition and chemical state of the elements. Surface concentrations of the elements were estimated based on the intensity of the corresponding core-level spectra with consideration of atomic sensitivity factors.[70] Curve fitting was performed with a combination of Gaussian and Lorentzian functions after Shirley background subtraction. Spectra were processed using the XPS-Calc program tested previously on a number of catalytic systems.[71–73]

X-ray Absorption near Edge spectra and X-ray Absorption Fine Structure

X-ray absorption near edge structure (XANES) spectra at Pt L_3 absorption edge were recorded ex situ at the SUL-X beamline of the KIT synchrotron radiation source (Karlsruhe, Germany) in transmission mode. Catalyst samples were measured as powders packed in Kapton tubes (d = 1.6 mm). The spectra were corrected for the energy shift using a spectrum of Pt foil measured simultaneously and then normalized using the Athena program from the IFFEFIT software package.[74] The average Pt oxidation state was determined from an average number of oxygen atoms in the first coordination shell of Pt as obtained during the analysis of extended X-ray absorption fine structure (EXAFS). For this purpose EXAFS spectra were background-subtracted, k^2-weighted and Fourier-transformed in the k-range 2.5–10.5 $Å^{-1}$ and multiplied by a Hanning window with sill size of 1 $Å^{-1}$. The amplitude reduction factor $S_0^2 = 0.96$ was obtained by fitting PtO_2 (Alfa Aesar, 99.95%) reference spectrum to a structural model reported in the Inorganic Crystal Structure Database (ICSD, CC = 4415). The fits were performed using Artemis[74] by a least square method in R-space between 1.0 and 2.5 Å in the case of a single O shell and between 1.0 and 3.0 Å when fitting O and Pt (metallic) shells. Coordination numbers, interatomic distances, energy shift (δE_0) and mean square deviation of interatomic distances (σ^2) were refined during the fitting. The absolute misfit between theory and experiment was expressed by ρ.

For the *operando* experiments the catalysts (approx. 5 mg, pressed and sieved to 100–200 μm grains) were placed in *in situ* microreactors (quartz capillary, 1.5 mm diameter, 20 μm wall thickness, Hilgenberg GmbH) heated by a hot air blower.[75,76] X-rays probed the first 1 mm of catalyst near the inlet of the catalyst bed. Gases were dosed using mass flow controllers and the outlet gas was analyzed using an MKS MultiGas 2030 FTIR gas analyzer. The concentration of the produced N_2 was not measured directly but determined as a difference between the reacted NH_3 and produced NO, NO_2, and N_2O taking into account the number of N atoms in each of these species. The total gas flow was 70 cm^3/min and the Gas Hourly Space Velocity (GHSV) – 630 000 h^{-1}. As-prepared catalysts were heated twice in flow of 890 ppm NH_3 and 10 vol.% O_2 (He and N_2 mixture as balance) from 50 °C to 400 °C (ramp to setpoint 5 °C/min, cooling down between heating in the same gas feed). *Pt-N-400* and *Pt-N-400-250H* were measured at P64 beamline of the PETRA III synchrotron (DESY, Hamburg, Germany) operating in the QEXAFS mode. The average Pt oxidation state was determined by a linear combination analysis (LCA) of the XANES spectra using internal references from QEXAFS datasets in a fitting range of 11544–11594 eV using JAQ software.[77] To translate the relative fractions obtained from the QEXAFS analysis to the oxidation state of Pt the internal reference spectra were exported and evaluated using LCA with Pt foil and PtO_2 reference spectra in Athena.

Catalytic Measurements

The catalytic measurements were carried out using an automatic setup equipped with a plug flow quartz reactor (i.d. = 9 mm), FTIR spectrometer (I1801, MIDAC corp., USA) and a gas chromatograph (Crystal 2000 M, CHROMATEC). The catalyst weight was 0.145 g. The reaction mixture containing 0.1 vol.% NH_3, 4.0 vol.% O_2 (balance He) was introduced at a rate of 500 cm^3/min and GHSV – 120 000 h^{-1}. Each sample was heated twice in the $NH_3 + O_2$ mixture from room temperature to 400 °C at a heating rate of 10 °C/min. Catalytic data obtained during the second heating in the reaction mixture are presented. Concentrations of NH_3, N_2O, NO, and NO_2 were measured by gas-phase FTIR spectroscopy, while the amounts of N_2 and O_2 were defined using the gas chromatography. Ammonia conversion (in %) was calculated as $(C_{in}\text{-}C_{out})/C_{in} \cdot 100$, where C_{in} – inlet NH_3 concentration and C_{out} – outlet NH_3 concentration. The product selectivity (S_i) was calculated as $n_i/\Sigma n_i$, where n_i – the concentration of the reaction product (N_2, N_2O, NO, or NO_2).

Temperature Programmed Adsorption of NH_3 (TPD-NH_3)

Before the TPD-NH_3 experiment, 0.25 g of each sample was outgassed in He flow at 400 °C for 2 h followed by cooling to room temperature (27 ± 2 °C). Then, the sample was treated with 0.1% NH_3/He mixture up to complete ammonia saturation. Afterward the system was flushed with 500 cm^3/min He flow to a residual NH_3 concentration below 5 ppm. Finally, the sample was heated to 400 °C with a ramp rate of 10 °C/min. NH_3 was detected by the combination of FTIR and GC during desorption.

Acknowledgments

The work was supported by Helmholtz – Russian Science Foundation Joint Research Groups grant #18-43-06201 from 03.09.2018 (RSF)/HRSF-0046 from 01.09.2018 (HGF). We acknowledge DESY (Hamburg, Germany), a member of the Helmholtz Association HGF, for the provided beamtime. Parts of this research were carried out at PETRA III and we would like to thank Dr. Edmund Welter, Dr. Wolfgang Caliebe, and Dr. Vadim Murzin for assistance in using beamlines P64 and P65. In addition, we thank the Institute for Beam Physics and Technology (IBPT) for the operation of the storage ring, the Karlsruhe Research Accelerator (KARA) at KIT (Karlsruhe, Germany), in particular Dr. Jörg Göttlicher and Dr. Ralph Steininger for their help and technical support during experiments at SUL-X beamline of the Institute for Photon Science and Synchrotron Radiation (IPS).

Conflict of Interest

The authors declare no conflict of interest.

Keywords: ammonia slip catalyst · NH_3 · operando spectroscopy · Pt/Al_2O_3 · platinum

[1] A. Walker, *Top. Catal.* **2016**, *59*, 695–707.
[2] T. Johnson, *SAE Int. J. Engines* **2016**, *9*, 1258–1275.
[3] R. Kraehnert, M. Baerns, *Chem. Eng. J.* **2008**, *137*, 361–375.
[4] R. Burch, B. W. L. Southward, *J. Catal.* **2000**, *195*, 217–226.
[5] B. Bahrami, V. G. Komvokis, M. S. Ziebarth, O. S. Alexeev, M. D. Amiridis, *Appl. Catal. B* **2013**, *130*, 25–35.
[6] R. Zhang, N. Liu, Z. Lei, B. Chen, *Chem. Rev.* **2016**, *116*, 3658–3721.
[7] H. Wu, Z. Ma, Z. Lin, H. Song, S. Yan, Y. Shi, *Nanomaterials* **2019**, *9*, 388.
[8] A. De Marco, C. Proietti, A. Anav, L. Ciancarella, I. D'Elia, S. Fares, M. F. Fornasier, L. Fusaro, M. Gualtieri, F. Manes, *Environ. Int.* **2019**, *125*, 320–333.
[9] Y. Pan, S. Tian, D. Liu, Y. Fang, X. Zhu, Q. Zhang, B. Zheng, G. Michalski, Y. Wang, *Environ. Sci. Technol.* **2016**, *50*, 8049–8056.
[10] L. Chmielarz, M. Jabłońska, *RSC Adv.* **2015**, *5*, 43408–43431.
[11] D. Chakraborty, H. N. Petersen, C. Elkjær, A. Cagulada, T. Johannessen, *Fuel Cells Bull.* **2009**, *2009*, 12–15.
[12] S. Z. Andersen, V. Čolić, S. Yang, J. A. Schwalbe, A. C. Nielander, J. M. McEnaney, K. Enemark-Rasmussen, J. G. Baker, A. R. Singh, B. A. Rohr, *Nature* **2019**, *570*, 504–508.
[13] Z. W. She, J. Kibsgaard, C. F. Dickens, I. Chorkendorff, J. K. Nørskov, T. F. Jaramillo, *Science* **2017**, *355*, eaad4998.
[14] D. Chakraborty, C. D. Damsgaard, H. Silva, C. Conradsen, J. L. Olsen, H. W. P. Carvalho, B. Mutz, T. Bligaard, M. J. Hoffmann, J.-D. Grunwaldt, *Angew. Chem. Int. Ed.* **2017**, *56*, 8711–8715; *Angew. Chem.* **2017**, *129*, 8837–8841.
[15] M. Colombo, I. Nova, E. Tronconi, V. Schmeißer, B. Bandl-Konrad, L. Zimmermann, *Appl. Catal. B* **2013**, *142*, 861–876.
[16] K. Kamasamudram, N. Currier, M. Castagnola, H. Chen, *SAE Int. J. Engines* **2011**, *4*, 1810–1821.
[17] S. Shrestha, M. P. Harold, K. Kamasamudram, A. Kumar, L. Olsson, K. Leistner, *Catal. Today* **2016**, *267*, 130–144.
[18] A. Scheuer, W. Hauptmann, A. Drochner, J. Gieshoff, H. Vogel, M. Votsmeier, *Appl. Catal. B* **2012**, *111*, 445–455.
[19] M. A. Smith, K. Kamasamudram, T. Szailer, A. Kumar, A. Yezerets, *SAE Tech. Pap. Ser.* **2014**, *1*, 1–6.
[20] D. P. Sobczyk, E. J. M. Hensen, A. M. De Jong, R. A. Van Santen, *Top. Catal.* **2003**, *23*, 109–117.
[21] W. D. Mieher, W. Ho, *Surf. Sci.* **1995**, *322*, 151–167.
[22] E. V. Rebrov, M. H. J. M. De Croon, J. C. Schouten, *Chem. Eng. J.* **2002**, *90*, 61–76.
[23] J. Pérez-Ramírez, E. V. Kondratenko, V. A. Kondratenko, M. Baerns, *J. Catal.* **2004**, *227*, 90–100.
[24] A. C. M. Van Den Broek, J. Van Grondelle, R. A. Van Santen, *J. Catal.* **1999**, *185*, 297–306.
[25] T. K. Hansen, Development of New Diesel Oxidation and NH_3 Slip Catalysts, Technical University of Denmark (DTU), **2017**.
[26] A. Y. Stakheev, D. A. Bokarev, I. P. Prosvirin, V. I. Bukhtiyarov, in *Adv. Nanomater. Catal. Energy*, Elsevier Inc., **2018**, pp. 295–320.
[27] J. J. Ostermaier, J. R. Katzer, W. H. Manogue, *J. Catal.* **1974**, *33*, 457–473.
[28] D. A. Svintsitskiy, E. M. Slavinskaya, O. A. Stonkus, A. V. Romanenko, A. I. Stadnichenko, L. S. Kibis, E. A. Derevyannikova, A. A. Evtushkova, A. I. Boronin, *J. Struct. Chem.* **2019**, *60*, 919–931.
[29] A. C. M. Van den Broek, Low Temperature Oxidation of Ammonia over Platinum and Iridium Catalysts, Technische Universiteit Eindhoven, **1998**.
[30] D. P. Sobczyk, J. Van Grondelle, P. C. Thüne, I.E. Kieft, A. M. De Jong, R. A. Van Santen, *J. Catal.* **2004**, *225*, 466–478.
[31] E. Marceau, M. Che, J. Saint-Just, J. M. Tatibouët, *Catal. Today* **1996**, *29*, 415–419.
[32] H. Lieske, G. Lietz, H. Spindler, J. Völter, *J. Catal.* **1983**, *81*, 8–16.
[33] O. B. Bel'skaya, R. K. Karymova, D. I. Kochubei, V. K. Duplyakin, *Kinet. Catal.* **2008**, *49*, 729–736.
[34] R. M. Mironenko, O. B. Belskaya, V. P. Talsi, T. I. Gulyaeva, M. O. Kazakov, A. I. Nizovskii, A. V. Kalinkin, V. I. Bukhtiyarov, A. V. Lavrenov, V. A. Likholobov, *Appl. Catal. A* **2014**, *469*, 472–482.
[35] E. Ogel, M. Casapu, D. E. Doronkin, R. Popescu, H. Störmer, C. Mechler, G. Marzun, S. Barcikowski, M. Türk, J.-D. Grunwaldt, *J. Phys. Chem. C* **2019**, *123*, 5433–5446.
[36] A. C. M. Van den Broek, J. Van Grondelle, R. A. Van Santen, *Catal. Lett.* **1998**, *55*, 79–82.
[37] G. Olofsson, L. R. Wallenberg, A. Andersson, *J. Catal.* **2005**, *230*, 1–13.
[38] A. Boubnov, S. Dahl, E. Johnson, A. P. Molina, S. B. Simonsen, F. M. Cano, S. Helveg, L. J. Lemus-Yegres, J.-D. Grunwaldt, *Appl. Catal. B* **2012**, *126*, 315–325.
[39] A. Chakrabarti, M. E. Ford, D. Gregory, R. Hu, C. J. Keturakis, S. Lwin, Y. Tang, Z. Yang, M. Zhu, M. A. Bañares, *Catal. Today* **2017**, *283*, 27–53.
[40] F. Wang, J. Jiang, B. Wang, *Catalysts* **2019**, *9*, 477.
[41] G. Novell-Leruth, J. M. Ricart, J. Pérez-Ramírez, *J. Phys. Chem. C* **2008**, *112*, 13554–13562.
[42] J. Schäffer, V. A. Kondratenko, N. Steinfeldt, M. Sebek, E. V. Kondratenko, *J. Catal.* **2013**, *301*, 210–216.
[43] M. Peuchert, H. P. Bonzel, *Surf. Sci.* **1984**, *145*, 239–259.
[44] Z. R. Ismagilov, S. A. Yashnik, A. N. Startsev, A. I. Boronin, A. I. Stadnichenko, V. V. Kriventsov, S. Kasztelan, D. Guillaume, M. Makkee, J. A. Moulijn, *Catal. Today* **2009**, *144*, 235–250.
[45] D. A. Svintsitskiy, L. S. Kibis, A. I. Stadnichenko, S. V. Koscheev, V. I. Zaikovskii, A. I. Boronin, *ChemPhysChem* **2015**, *16*, 3318–3324.
[46] A. V. Kalinkin, M. Y. Smirnov, A. I. Nizovskii, V. I. Bukhtiyarov, *J. Electron Spectrosc. Relat. Phenom.* **2010**, *177*, 15–18.
[47] Y. T. Kim, K. Ohshima, K. Higashimine, T. Uruga, M. Takata, H. Suematsu, T. Mitani, *Angew. Chem. Int. Ed.* **2006**, *45*, 407–411; *Angew. Chem.* **2006**, *118*, 421–425.
[48] E. I. Vovk, A. V. Kalinkin, M. Y. Smirnov, I. O. Klembovskii, V. I. Bukhtiyarov, *J. Phys. Chem. C* **2017**, *121*, 17297–17304.
[49] J. E. Drawdy, G. B. Hoflund, S. D. Gardner, E. Yngvadottir, D. R. Schryer, *Surf. Interface Anal.* **1990**, *16*, 369–374.
[50] F. J. Gracia, E. E. Wolf, J. T. Miller, A. J. Kropf, *Stud. Surf. Sci. Catal.* **2001**, *139*, 471–478.
[51] T. I. Hyde, P. W. Ash, D. A. Boyd, G. Randlshofer, K. Rothenbacher, G. Sankar, *Platinum Met. Rev.* **2011**, *55*, 233–245.
[52] G.-W. Jang, K. Rajeshwa, *J. Electrochem. Soc.* **1987**, *134*, 1830–1835.
[53] C. Sakthivel, L. Keerthana, I. Prabha, *Johnson Matthey Technol. Rev.* **2019**, *63*, 122–133.
[54] A. Boubnov, A. Gänzler, S. Conrad, M. Casapu, J.-D. Grunwaldt, *Top. Catal.* **2013**, *56*, 333–338.
[55] D. A. Svintsitskiy, L. S. Kibis, A. I. Stadnichenko, E. M. Slavinskaya, A. S. Zaguzin, A. V. Romanenko, E. A. Derevyannikova, O. A. Stonkus, A. I. Boronin, in *AIP Conf. Proc.*, **2019**, p. 20028.
[56] A. M. Gänzler, M. Casapu, A. Boubnov, O. Müller, S. Conrad, H. Lichtenberg, R. Frahm, J.-D. Grunwaldt, *J. Catal.* **2015**, *328*, 216–224.
[57] A. Arvajová, P. Kočí, *Chem. Eng. Sci.* **2017**, *158*, 181–187.
[58] L. Olsson, H. Karlsson, *Catal. Today* **2009**, *147*, 12–15.
[59] L. Zhang, H. He, *J. Catal.* **2009**, *268*, 18–25.
[60] L. Gang, B. G. Anderson, J. Van Grondelle, R. A. Van Santen, *Appl. Catal. B* **2003**, *40*, 101–110.

[61] D. P. Sobczyk, A. M. De Jong, E. J. M. Hensen, R. A. Van Santen, *J. Catal.* **2003**, *219*, 156–166.
[62] R. W. McCabe, C. Wong, H. S. Woo, *J. Catal.* **1988**, *114*, 354–367.
[63] E. Marceau, H. Lauron-Pernot, M. Che, *J. Catal.* **2001**, *197*, 394–405.
[64] P. Berteau, B. Delmon, *Catal. Today* **1989**, *5*, 121–137.
[65] C.-B. Wang, C.-T. Yeh, *J. Catal.* **1998**, *178*, 450.
[66] A. Arvajová, P. Kočí, V. Schmeißer, M. Weibel, *Appl. Catal. B* **2016**, *181*, 644–650.
[67] N. Seriani, Z. Jin, W. Pompe, L. C. Ciacchi, *Phys. Rev. B* **2007**, *76*, 1–10.
[68] *TOPAS, version 4.2., Bruker AXS Inc., 2009, Madison, Wisconsin, USA*.
[69] M. D. Abramoff, P. J. Magalhaes, J. S. Ram, *Biophotonics Int.* **2004**, *11*, 36–42.
[70] J. F. Moulder, W. F. Stickle, P. E. Sobol, K. D. Bomben, *Handbook of X-Ray Photoelectron Spectroscopy*, Perkin-Elmer Corp, Eden Prairie, Minnesota, USA, **1992**.
[71] L. S. Kibis, D. A. Svintsitskiy, T. Y. Kardash, E. M. Slavinskaya, E. Y. Gotovtseva, V. A. Svetlichnyi, A. I. Boronin, *Appl. Catal. A* **2019**, *570*, 51–61.
[72] E. D. Grayfer, L. S. Kibis, A. I. Stadnichenko, O. Y. Vilkov, A. I. Boronin, E. M. Slavinskaya, O. A. Stonkus, V. E. Fedorov, *Carbon N. Y.* **2015**, *89*, 290–299.
[73] D. A. Svintsitskiy, E. M. Slavinskaya, T. Y. Kardash, V. I. Avdeev, B. V. Senkovskiy, S. V. Koscheev, A. I. Boronin, *Appl. Catal. A* **2016**, *510*, 64–73.
[74] B. Ravel, M. Newville, *J. Synchrotron Radiat.* **2005**, *12*, 537–541.
[75] J.-D. Grunwaldt, N. Van Vegten, A. Baiker, *Chem. Commun.* **2007**, 4635–4637.
[76] D. E. Doronkin, H. Lichtenberg, J.-D. Grunwaldt, in *XAFS Tech. Catal. Nanomater. Surfaces*, **2016**, pp. 75–89.
[77] B. Bornmann, J. Kläs, O. Müller, D. Lützenkirchen-Hecht, R. Frahm, *AIP Conf. Proc.* **2019**, *2054*, 40008.

Manuscript received: September 11, 2019
Revised manuscript received: October 15, 2019
Accepted manuscript online: October 15, 2019
Version of record online: ■■, ■■■

FULL PAPERS

Ammonia shall not pass: Metallic Pt is the most active in NH_3 oxidation at $T < 200\,^{\circ}C$ on Pt/Al_2O_3. The surface of Pt nanoparticles was found to be oxidized under NH_3 oxidation conditions, leading to the formation of undesirable products. The presence of Cl on the catalyst surface hinders Pt reduction decreasing catalyst activity.

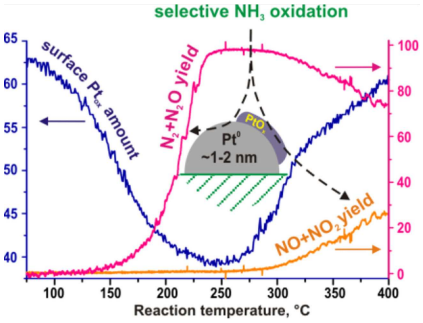

Dr. D. A. Svintsitskiy, Dr. L. S. Kibis, Dr. A. I. Stadnichenko, Dr. E. M. Slavinskaya, Dr. A. V. Romanenko, E. A. Fedorova, Dr. O. A. Stonkus, Dr. D. E. Doronkin, V. Marchuk, Dr. A. Zimina, Dr. M. Casapu, Prof. J.-D. Grunwaldt, Prof. A. I. Boronin**